Structures of Active and Latent PAI-1: A Possible Stabilizing Role for Chloride Ions‡

Thomas J. Stout,*,§ Hugh Graham,§ Douglas I. Buckley,§ and David J. Matthews*,§

MetaXen, 280 East Grand Avenue, South San Francisco, California 94080

Received February 7, 2000; Revised Manuscript Received May 9, 2000

ABSTRACT: Serpins exhibit a range of physiological roles and can contribute to certain disease states dependent on their various conformations. Understanding the mechanisms of the large-scale conformational reorganizations of serpins may lead to a better understanding of their roles in various cardiovascular diseases. We have studied the serpin, plasminogen activator inhibitor 1 (PAI-1), in both the active and the latent state and found that anionic halide ions may play a role in the active-to-latent structural transition. Crystallographic analysis of a stable mutant form of active PAI-1 identified an anion-binding site between the central β-sheet and a small surface domain. A chloride ion was modeled in this site, and its identity was confirmed by soaking crystals in a bromide-containing solution and calculating a crystallographic difference map. The anion thus located forms a 4-fold ligated linchpin that tethers the surface domain to the central β-sheet into which the reactive center loop must insert during the active-to-latent transition. Timecourse experiments measuring active PAI-1 stability in the presence of various halide ions showed a clear trend for stabilization of the active form with $F^- > Cl^- > Br^- \gg I^-$. We propose that the "stickiness" of this pin (i.e., the electronegativity of the anion) contributes to the energetics of the active-to-latent transition in the PAI-1 serpin.

Plasminogen activator inhibitor-1 (PAI-1)[1] is a 379-amino acid glycoprotein of the circulatory system that plays a crucial role in the regulation of fibrinolysis and has also been implicated in several other crucial biological processes including tumor invasion, neovascularization, inflammation, and wound healing (*1*−*4*). PAI-1 is the principal physiological regulator of both tissue-type plasminogen activator (t-PA) and urinary-type plasminogen activator (u-PA) (*1*, *2*) and is a member of the superfamily of serine protease inhibitors (serpins).

Serpins form a large family of homologous proteins that share ∼35% sequence homology (*5*−*9*) as well as a common fold.[2] Like other inhibitory serpins, PAI-1 forms a 1:1 stoichiometric complex with its target protease (t-PA), followed by the rapid formation of a covalent bond between the protease active site serine hydroxyl and the main-chain carbonyl of the inhibitor P1 reactive center residue (*10*−*12*). Once t-PA has carried out this main-chain cleavage at PAI-1's reactive center, the covalent complex undergoes a dramatic conformational rearrangement into a long-term stable form (*13*−*15*). Under certain conditions, this transition does not proceed, and the covalent complex undergoes hydrolysis of the acyl−enzyme bond, thereby behaving like a peptidic substrate (*16*−*19*). However, the physiological relevance of this substrate form of PAI-1 is unclear.

PAI-1 is an unusual serpin in that the active, inhibitory conformation is relatively unstable. Under physiological conditions, human PAI-1 has a half-life of ∼2 h (*20*, *21*) and spontaneously converts to an inactive, "latent" form. The active-to-latent transition is manifest as a large conformational change, involving the insertion of the reactive center peptide loop (RCL) into the center of the primary β-sheet structure, which forms the core of the PAI-1 molecule (*22*) (Figure 1). As a result, the RCL is sequestered such that PAI-1 is no longer recognized or bound by t-PA. This lability of the PAI-1 active form is likely utilized as a regulatory element in the circulatory system to ensure proper response to rapidly changing fibrinolytic requirements. On the basis of active and latent-form crystal structures (Figure 1), we know the end points of this structural transition as well as the only pathway through which the mobile RCL must pass. In the active form, the RCL is an extended loop located above the upper domain where it serves as "bait" for the target protease. The N-terminal end of the RCL leads directly out of strand 5A of the central β-sheet on the "front" face of the protein as drawn in Figure 2, while the C-terminal end of the RCL returns into the body of the protein on the "back" face of the protein, leading into the β-sheet portion of the upper domain. During the structural transition from the active to the latent form, this extended loop begins to insert into the central β-sheet by forming a turn at the C-terminal end

‡ Coordinates have been deposited with the PDB under entry codes 1DVM and 1DVN.

* To whom correspondence should be addressed. E-mail: tstout@exelixis.com, matthews@exelixis.com.

§ Current Address: Exelixis, Inc., 280 East Grand Avenue, South San Francisco, CA 94080.

[1] Abbreviations: PAI-1, plasminogen activator inhibitor, type 1; t-PA, tissue-type plasminogen activator; u-PA, urinary-type plasminogen activator; SERPIN, serine protease inhibitor; PCR, polymerase chain reaction; PEG, poly(ethylene glycol); MPD, methylpentane diol; *l*-PAI-1, latent conformation of PAI-1; HTLI-PAI-1, stable active form of PAI-1; RCL, reactive center loop; NCS, noncrystallographic symmetry.

[2] Examples include ovalbumin, α-1-antitrypsin, antithrombin III, α-1-antichymotrypsin, leukocyte elastase inhibitor, plankalbumin, kallistatin, maspin, and alaserpin, among others.

10.1021/bi000290w CCC: $19.00
Published on Web 06/30/2000

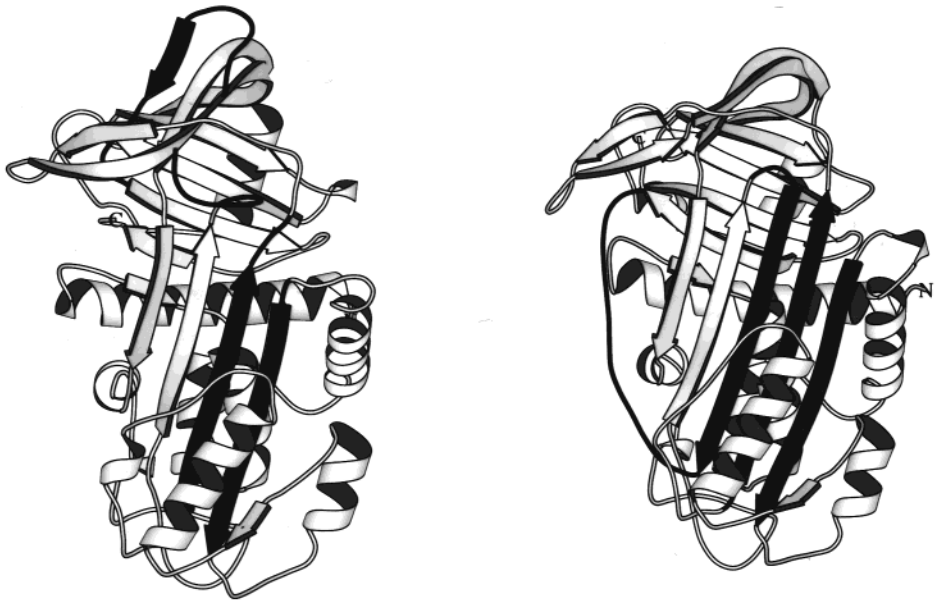

FIGURE 1: Comparison of active (left) and latent (right) forms of PAI-1. The regions that undergo the largest conformational shifts are indicated in dark gray. These include the RCL (RCL: residues 331−357), which moves from an exposed position as "bait" for the target protease to a sequestered position as the central strand of the core β-sheet. This structural reordering requires movement of the RCL around the C-terminal face of the protein, outward shifting of strands 1A, 2A, and 3A, as well as a "hinging" motion by the small coil−turn−helix domain shown at the lower center of the structure.

of strand 5A. As this insertion progresses, two barriers are confronted. One involves unraveling of the short S1C strand and movement of the entire RCL loop around the upper domain past the C-terminus, much like a jump rope passing over the user's head. Several mutagenesis studies have identified crucial residues in the upper domain that served to either accelerate or retard the ability of the RCL to pass over this surface of the protein (*23*, *24*). The other transitional barrier involves the need to displace a small domain (residues 128−161; Figure 2) that sits atop the central β-sheet, so that the RCL can continue its insertion into the β-sheet. This small domain is only directly threaded into the main fold through connections at the bottom of the domain and so is able to fold away from the main body of the protein in a hinging motion. Thus, we have termed this the "hinge domain" (Figure 2).

Although the active-to-latent transition occurs spontaneously in wild-type PAI-1, a number of factors have been found to stabilize the active form. Lowering the pH of the buffer dramatically increases the half-life of the active form (*18*). It has been proposed that the stabilizing effect of low pH may be due to an ionizable group with a pK_a of ~6, possibly His143 (*28*). Moreover, arginine has been shown to stabilize the active form of PAI-1 (*18*, *29*). It has been suggested that this effect may be related to the physiological stabilization of PAI-1 by its interaction with vitronectin (*29*), since arginine residues are implicated in the binding interface between PAI-1 and vitronectin. Increasing the concentration of NaCl from 50 mM to 1 M also dramatically increases the half-life of the active form (*18*). However, despite the above advances in our understanding of the active-to-latent transition, the role of NaCl in stabilizing PAI-1 has remained unclear.

As part of our effort to understand the mechanistic biology of human PAI-1, we have solved and refined to high-resolution the crystal structures of both the latent and a stable-active form of PAI-1. The literature contains reports of crystal structure determinations of each of these species, although at moderate resolutions [latent: 2.8 Å (*22*); active: ~3.0 Å (*30*)]. We report here crystallographic determinations of both the latent and an active-form tetramutant of PAI-1 at substantially higher resolutions (2.1 and 2.4 Å, respectively). Many additional details of these structures have been observed from the higher resolution data and are discussed below. In particular, a chloride-binding site has been identified at a central location in the structure, implying a stabilizing role for physiological salt in the activity of PAI-1. This chloride ion was shown to be displaced in crystallographic studies by bromide, and the anion binding site in general was shown to modulate the stability of the wild-type active conformation through replacement with the entire halide series: F^-, Cl^-, Br^-, and I^-. Coupled with previous studies (*23*, *25*−*27*) showing that stabilization of the active conformation of PAI-1 can be readily introduced through mutagenesis, it is proposed that PAI-1 has evolved a physiologically required metastability. This metastability is tightly regulated both externally through interactions with partner proteins (e.g., vitronectin), and perhaps internally as well, through this anion-binding site that serves to hold a displaceable "pin" holding the hinge domain in place.

MATERIALS AND METHODS

Cloning, Expression, and Purification. The PAI-1 gene was cloned by PCR from a human umbilical vein endothelium library (Stratagene, La Jolla, CA), and the sequence was confirmed using a Li-cor 4200 DNA sequencer (Li-cor, Lincoln, NE). On the basis of previous work by Sancho et al. (*31*), the 5′ DNA sequence was modified to include *Escherichia coli*-preferred codons as follows: wt: GTG CAC CAT CCC CCA TCC TAC GTG ... and 5′-modified: GTA CAT CAT CCA CCG AGC TAT GTT ...

The gene was cloned between the *Nco*I and *Hin*dIII sites of the pTrcHis2A expression vector (Invitrogen, Carlsbad,

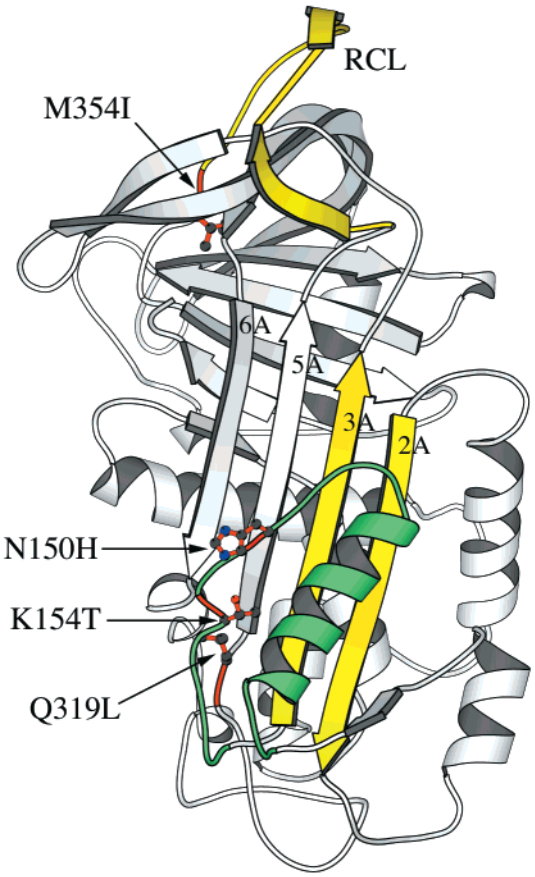

FIGURE 2: Structure of the active form of human PAI-1. Locations of the four mutations that confer extended stability to the active conformation are shown in red and labeled accordingly. The RCL (shown in yellow) extends away from the protein, and in two of four independent molecules in the crystal structure, forms interactions with adjacent PAI-1 molecules. The strands that slide outward to accommodate the incoming RCL during the active → latent transition are also shown in yellow. The "hinge domain", which folds away from the surface of the central β-sheet to allow the RCL to insert into the central β-sheet, is shown in green and includes residues 128−161.

CA), directing expression of full-length PAI-1 with an N-terminal methionine residue. For the stable-active mutant [HTLI-PAI-1 (*25*)], mutations N150**H** (AAC → CAC), K154**T** (AAA → ACA), Q319**L** (CAG → CTG), and M354**I** (ATG → ATC) were introduced by PCR.

Protein was expressed in *E. coli* XL-1 Blue (Stratagene, La Jolla, CA) using a 5L Biostat B fermentor (B. Braun Biotech, Allentown, PA). A complex medium (2×TY broth containing 1 g/L glucose and 50 μg/mL ampicillin) was inoculated with an overnight LB culture (3−5% of the final fermentor volume) and grown at 37 °C, pH 7.0, to an OD_{600} of 0.7−0.8 AU, stirring at >120 rpm to keep the dissolved oxygen level above 30% of air saturation. IPTG was then added to a final concentration of 1 mM, and growth continued for 3−3.5 h, with 0.5 g/L glucose added when glucose levels were depleted. When OD_{600} reached 2.5−3.0 AU, the fermentor was rapidly chilled, and the broth was harvested. Cells were harvested by centrifugation at 4 °C, 5000 rpm for 25 min in a Sorvall RC-3B with an H6000A rotor (Kendro Lab. Products, Newton, CT).

Active and latent forms of PAI-1 were purified using a modification of the method of Kvassman and Shore (*32*). The cell pellet was resuspended in 3 vol of lysis buffer [50 mM $KHPO_4$, 1 mM EDTA, 80 mM $(NH_4)_2SO_4$, pH 6.5, containing 2 μg/mL aprotinin, 1 μg/mL pepstatin A, 2 μg/mL antipain, 1 μg/mL leupeptin, 1 μg/mL chymostatin and 1 mM PMSF], homogenized using a hand-held homogenizer (Virtis, Gardiner, NY) and lysed using two passes at 16 000 psi in a microfluidizer (Microfluidics Corp., Newton, MA). Benzamidine was immediately added to 1 mM, and the lysate was centrifuged at 20000*g* for 20 min. The supernatant (containing PAI-1) was precipitated with 1.05 vol of saturated $(NH_4)_2SO_4$ on ice for 30 min, then centrifuged for 25 min at 20000*g*. The pellet was resuspended in 50 mM $KHPO_4$ and 1 mM EDTA, pH 6.5, and purified using a BioCAD 700 E system (PE Biosystems, Foster City, CA). Initial load was onto a DEAE Sephacel (Pharmacia Biotech, Uppsala, Sweden) precolumn followed by an SP Sepharose HP column (Pharmacia) from which the protein was eluted with a 4 column volume salt gradient from 0.08 to 0.5 M $(NH_4)_2SO_4$. Active and latent forms of PAI-1 were separated by loading the peak fractions containing PAI-1 (made to 1.15 M in $(NH_4)_2SO_4$) onto a Toyopearl Phenyl 650s column (TosoHaas, Montgomeryville, PA) from which it was eluted with a 5 column volume salt gradient to 0 M $(NH_4)_2SO_4$. Phosphate, EDTA, and pH levels were constant throughout the purification. Fractions were chilled on ice and assayed by SDS−PAGE for purity. Selected fractions were precipitated overnight against solid $(NH_4)_2SO_4$ at 4 °C. The precipitate was stored at 4 °C until needed and then redissolved in 50 mM phosphate buffer, pH 6.5, and buffer-exchanged into crystallization or assay buffers by gel filtration on a PD-10 column (Pharmacia Biotech, Uppsala, Sweden).

Crystallization. (1) Latent-PAI-1. Crystals of the latent form of PAI-1 (*l*-PAI) were grown by the hanging-drop vapor diffusion technique in Linbro multi-well tissue culture plates. Protein was used at ∼4 mg/mL in 50 mM Tris, pH 6.9, and 50 mM $MgSO_4$. Hanging drops were set up on silanized coverslips using 3 μL protein solution volumes, to which an equal volume of well solution was added before sealing the well. The well solution consisted of 1 mL of 2−8% PEG1000, 20 mM Tris (pH 8−8.4), and 1.5% MPD. Irregular platelike crystals grew within 1 week and typically reached a maximum size of 750 × 400 × 80 μm.

(2) HTLI-PAI-1. Crystals of the active form of PAI-1 were also grown in hanging drops, using a slightly different protocol. The protein was used at ∼11 mg/mL in 20 mM MES buffer, pH 6.1, and 1 M NaCl. Hanging drops were set up on silanized cover slips using 3−5 μL drops to which no well solution was added. Well solutions ranged from 1.7 to 2.0 M NaCl. Crystals appeared in 10−12 days and grew to full size in approximately 21 days. Many crystals grew as plate clusters; however, occasional single crystals grew as elongated plates exceeding 1 mm in the largest dimension. Crystals of HTLI-PAI were harvested, washed, dissolved, and assayed for activity against t-PA; the protein was shown to be fully active within the limits of the experiment (data not shown).

Data Collection. (1) Latent PAI-1. Diffraction data were collected to 2.0 Å resolution from a single 0.15 × 0.35 × 0.8 mm crystal at −178 °C. Prior to data collection, a single crystal was removed from the growth solution and placed in a cryo-protectant solution consisting of the well solution plus 5 % MPD. The crystal remained bathed in the cryo-

Table 1: Crystallographic Statistics[a]

	l-PAI	HTLI-PAI-1	HTLI-PAI-1 + NaBr
a (Å)	154.58	64.76	64.95
b	46.70	74.67	74.90
c	61.97	103.45	102.87
α (deg)		85.19	91.0
β	107.12	86.17	93.6
γ		64.34	115.7
space group	*C*2	*P*1	*P*1
Z	4	4	4
resolution	2.1	2.4	2.1
$<I/\sigma(I)>$	12.6(3.1)	7.6(2.4)	7.1(1.6)
R_{sym}	0.12(0.34)	0.093(0.221)	0.082(0.27)
total measurements	292 887	211 004	210 800
unique reflections	24 992	67 997	82 405
completeness	96.0(92.2)	88.8(78.4)	83.6(66.3)
ave redundancy	4.7	3.1	3.0
Refinement			
R factor	0.204	0.175	
R_{free} (5%)	0.269	0.271	
RMS deviations (geometry)			
bond lengths (Å)	0.006	0.009	
bond angles (deg)	1.2	1.5	

[a]Highest resolution bin values in parentheses.

protectant solution only long enough to move it away from the original mother liquor and form a new film in the mounting loop, a total of approximately 5−10 s. The crystal was then immediately placed in a cold N_2 gas stream. All data were collected in-house using Cu K_α radiation (λ = 1.54 Å) on an R-Axis IIc image plate detector. X-rays were generated with a Rigaku RU-H3R generator operating at 50 kV and 100 mA. The crystal-to-detector distance was 100 mm. Exposures were for 20 min per 1° of oscillation in Φ. A total of 180° of data were collected. The diffraction data were indexed, integrated, and scaled in spacegroup *C*2 with the HKL suite of programs (*33*). As indicated in Table 1, the overall R_{sym} = 0.12 (0.34 in the highest resolution bin) with $<I/\sigma(I)>$ = 12.6(3.1) and ∼5-fold average redundancy.

(2) HTLI−PAI-1. Diffraction data were collected to beyond 2.0 Å resolution from a single 0.08 × 0.4 × 0.8 mm crystal at −178 °C. Prior to data collection, a single crystal was removed from the growth solution and placed in a cryo-protectant solution consisting of the well solution plus 35% ethylene glycol. The crystal mounting and data collection procedures were the same as described above. A total of 270° of data were collected. The diffraction data were indexed, integrated, and scaled in spacegroup *P*1 with the HKL suite of programs (*33*). As shown in Table 1, the overall R_{sym} = 0.093(0.221) with $<I/\sigma(I)>$ = 7.6(2.4) and ∼3-fold average redundancy.

(3) Bromide Substitution. Diffraction data were collected to 2.1 Å resolution from a single 0.1 × 0.3 × 0.6 mm crystal at −178 °C. Prior to data collection, a single crystal of HTLI-PAI-1 was removed from the growth solution and placed in a cryo-protectant solution consisting of 35% ethylene glycol added to 2 M NaBr, rather than NaCl. The crystal was allowed to soak in the cryo-protectant solution for 5 min before being placed in a cold N_2 gas stream for data collection. Otherwise, the crystal mounting and data collection procedures were the same as described above. A total of 220° of data were collected. All diffraction data were indexed, integrated, and scaled in spacegroup *P*1 with the HKL suite of programs (*33*). As shown in Table 1, the overall R_{sym} = 0.087(0.272) with $<I/\sigma(I)>$ = 9.9(2.3) and ∼4-fold average redundancy.

Structure Solutions. (1) l-PAI-1. The structure of PAI-1 in the latent conformation was solved by molecular replacement using X-PLOR (*34*). The search probe was composed of coordinates derived from the previously published model (*22*), which was solved and refined at 2.6 Å resolution. A single solution was found that was 25.1 σ above the noise; there were no incorrect solutions found. The initial *R* factor, prior to any refinement, was 0.362 (R_{free} = 0.368). A number of cycles of manual rebuilding and refinement brought the *R* factor to 0.204 (R_{free} = 0.269) for a model that consisted of 379/379 amino acids and 313 molecules of ordered solvent. Refinement was done in X-PLOR using all data [30−2.1 Å, F ≥ 0σ(F)] to which a bulk-solvent correction had been applied.

(2) HTLI-PAI-1. The structure of the tetramutant HTLI-PAI-1 crystallized in an active conformation was solved by molecular replacement using X-PLOR. The successful search probe was composed of a molecule of *l*-PAI-1 from which *β*-strands A4 (residues 330−344), A3 (162−175), and A2 (90−100) as well as the remainder of the reactive center loop (RCL) from residues 345−357 and several loops with large thermal parameters had been deleted. This search probe contained a total of 280/379 residues per PAI-1 molecule or 280/1516 residues per asymmetric unit, approximately 18% of the scattering-matter to be determined. Self-rotation Patterson maps clearly indicated two independent two-folds that were approximately 80 and 65% of the maximum peak height corresponding to the identity matrix, indicating that these were noncrystallographic operators relating four non-equivalent copies in the asymmetric unit. The rotation function was solved by selecting the four signals in the top 10 peaks that adhered to the observed NCS operators. The positioning of all four molecules in the asymmetric unit was achieved in a build-up procedure, wherein one of the rotation function (RF) solutions was chosen to define the origin in space group *P*1, fixed in place, and the remaining three RF solutions were searched via the translation function (TF) to position each of them in the unit cell relative to that origin. The initial placement of four solutions in the unit cell gave an *R* factor = 0.505 and R_{free} = 0.503 for data between 8 and 3 Å. Refined NCS operators were derived from this molecular replacement solution, and all four molecules were treated as identical by NCS throughout the early rounds of structure building and refinement. After eight cycles of manual building and refinement (*R* factor = 0.332, R_{free} = 0.364), it became clear that regions of the four molecules within the asymmetric unit differed substantially, and the NCS constraints were removed. The subsequent building and refinement led to a fully refined structure with 1476 of 1516 residues located in defined electron density, 1636 molecules of ordered solvent, and 4 chloride ions (*R* factor = 0.175, R_{free} = 0.271). Refinement was done in X-PLOR using all data [30−2.4 Å, F ≥ 0σ(F)] to which a bulk-solvent correction had been applied.

(3) Bromide Substitution. The identity of the chloride ion was confirmed through replacement by bromide. Since the bromide soaked crystal was slightly nonisomorphous with the previously collected data, the difference map was calculated with the coordinates resulting from molecular

replacement, rather than a direct difference Fourier. Molecular replacement was performed with X-PLOR, searching with the four molecules of the asymmetric unit from which all water molecules had been removed but the four chloride ions retained. There was only one solution, at 34.2 σ above the noise. The initial *R* factor was 0.387. Rigid body refinement, defining each of the four molecules as an independent rigid body, brought the *R* factor to 0.324. At this point, a difference map was calculated using Fourier coefficients of F_o-F_c, Φ_{calc}. Each of the four anion binding sites showed strong positive difference peaks (7−15 σ), indicating additional unmodeled electron density in addition to the chloride ions already modeled at each site.

PAI-1 Stability Studies. Active wild-type PAI-1 was expressed and purified as described above and buffer-exchanged from 50 mM $KHPO_4$, pH 6.5, 1 mM EDTA into 10 mM Hepes, pH 7.4, 0.01% (w/w) Tween-20 containing 150 mM of either NaF, NaCl, NaBr, or NaI. Protein concentrations were estimated using a BCA protein assay kit (Pierce, Rockford, IL) with reference to a PAI-1 standard. Samples were diluted to 100 μg/mL in the appropriate buffer and incubated for 24 h at 25 °C or 30 min at 37 °C. PAI-1 activity was estimated at each timepoint by titration of PAI-1 samples against a fixed concentration of two-chain t-PA. One-chain t-PA (4×10^5 IU/mg) was obtained from Calbiochem (La Jolla, CA) and prepared as a 1 mg/mL solution in ammonium bicarbonate. Two-chain t-PA was prepared by diluting 13.15 μg of one-chain t-PA into 1.5 mL of assay buffer [10 mM Hepes, pH 7.4, 150 mM NaCl, and 0.01% (w/w) Tween-20] and incubating with 15 μL of 54 μg/mL human plasmin (American Diagnostica, Greenwich, CT) for 2 h at 25 °C. PAI-1 samples were diluted to appropriate concentrations in 100 μL of the above assay buffer and incubated with 5 μL of the two-chain t-PA preparation for 10 min at 25 °C in a 96-well polypropylene plate. A 67-μL aliquot of this solution was transferred to a clear plate containing 33 μL of 3 mM Pefachrome tPA substrate (Centerchem Inc., Stamford, CT), pre-warmed to 37 °C. t-PA activity was measured by monitoring the rate of *p*-nitroaniline formation at 405 nm over a period of 20 min at 37 °C.

RESULTS

Expression and Purification. Wild-type human PAI-1 and HTLI-PAI-1 were expressed and purified as described in Materials and Methods. Rapid cell growth was observed to continue postinduction and was required for consistent expression. Prolonged induction periods resulted in the formation of inclusion bodies, reducing the amount of soluble product available for purification; therefore, induction times were limited to 3−3.5 h. In addition, minimal medium growth produced cell growth but no protein expression, and high-density fed-batch fermentations were therefore not productive. Thermal lability of PAI-1 and its susceptibility to proteases also limited induction time and necessitated rapid cooling of the broth at harvest and the careful use of protease inhibitors to maximize yields. Final yields of up to 90 mg of protein were obtained from each 5-L fermentation using several purification runs, each yielding 15−40 mg of active protein. The active fraction of wild-type PAI-1 was typically 50 to 75% of total PAI-1; this fraction was much higher (>90%) for HTLI-PAI. SDS−PAGE analysis with Coomassie blue staining showed no detectable impurities in the major fraction of the eluted peaks, and fractions for further work were selected from this area.

Table 2: Structural Comparison of Structures

	l-PAI-1[a]	HTLI-PAI-1[b]
all α-carbons	1.39 Å	1.17
best subset (≤3.5 Å)	0.62	0.56
main chain	1.40	1.14
all atoms	1.94	1.48

[a] PDB code: 1C5G. [b] PDB code: 1B3K.

Crystallography − Latent PAI-1. Diffraction data were collected at −180 °C for the latent form of human PAI-1 and were processed to 2.1 Å resolution with good statistics. As indicated in Table 1, the overall $R_{sym} = 0.12$ (0.34 in the highest resolution bin) with $\langle I/\sigma(I)\rangle = 12.6(3.1)$ and ∼5-fold average redundancy. The structure was determined by molecular replacement as described (Materials and Methods) and refined to an *R* factor of 0.204 ($R_{free} = 0.269$) with good overall geometry and stereochemistry (Table 1). The crystal structure at 2.1 Å resolution is largely similar to that previously determined at 2.8 Å (*22*). A least-squares refined superposition of the two structures gave a root-mean-squared deviation (rmsd) of 1.39 Å on all α-carbons, and 0.62 Å for the best-fitting subset of 362 α-carbons (Table 2). The protein is of mixed α−β fold, principally dominated by a five-stranded β-sheet, the central strand of which (4A) is comprised of the RCL. The regions that differ most between the current structure and that previously reported principally involve surface-exposed loop regions. The more significant structural differences (pairwise C_α rmsds ≥ 1.0 Å) include F113−K122, P180−P200, T215−Y221, Y241−P246, A345−E351, and M377−P379. The first of these, F113−K122, forms the turn at the top of helix E and includes arginines 115 and 118 which, together with Arg76, have been implicated both in heparin binding (*35*, *36*) and possibly in the binding of low molecular weight inhibitors of PAI-1 activity (*37*). The region from A345−E351 includes the surface, random-coil region of the RCL that makes no specific interactions with the main body of the protein. The remainder of these regions of large deviation form a structural cluster, completely contained within the upper domain. There are large shifts in β-sheet C, as well as the connecting loops and the C-terminus. This region has been implicated through mutagenesis as playing a role in the stabilization of the active form, possibly through electrostatic interactions between β-sheet C and the RCL (*23*, *24*). Mottonen et al. (*22*) found that this region was located in poor electron density, and there is one gap of unmodeled structure for which there was insufficient electron density. In our study, all residues in this region have been located in good electron density, although they do display elevated thermal parameters relative to the rest of the structure, implying greater mobility.

Crystallography − Active PAI-1. Diffraction data were collected at −180 °C for an active form of human PAI-1 and were processed to 2.4 Å resolution with good statistics. As indicated in Table 1, the overall $R_{sym} = 0.093$ (0.221 in the highest resolution bin) with $\langle I/\sigma(I)\rangle = 7.6(2.4)$ and ∼3-fold average redundancy. The structure was determined by molecular replacement as described (Materials and Methods) and refined to an *R* factor of 0.175 ($R_{free} = 0.271$) with good

Table 3: Geometry around Chloride Ions

	A	B[a]	C[a]	D
		distances (Å)		
S149(N)	3.48	3.01	3.21	3.22
H150(N)	3.51	3.54	3.49	3.52
K323(Nζ)	2.69	3.33	3.18	3.47
K325(Nζ)	2.86	3.60		2.99
S149(Oγ1)		3.53		
H150(Nδ1)		3.21	3.36	
W783(OH2)			2.83	
W784(OH2)			3.11	
		angles (deg)		
323−Cl−325[b]	83.2	91.3	106.4[c]	83.7
323−Cl−150	104.4	88.3	95.7	123.6
325−Cl−149	111.7	113.3	98.4[c]	102.6
149−Cl−150	46.4	50.8	49.8	51.0

[a] Side chain of H150 is "in" toward the anion binding site. [b] For example, 323−Cl−325: K323(Nζ)−Cl−K325(Nζ). [c] Nζ position of K325 is replaced with water-784.

overall geometry and stereochemistry (Table 1). The general features of this structure are largely in agreement with the structure recently determined at a nominal 3 Å resolution by Sharp et al. (*30*) (Table 2), with the largest differences occurring in the RCL (330−343) and smaller differences in several turns (26−30, 192−196, 262−266, 310−315). Unlike the latent form, in the active conformation of PAI-1, the RCL protrudes from the main body of the protein and in two of the four independent molecules in the asymmetric unit forms an additional β-strand in sheet A with a neighboring PAI-1 molecule. In the other two molecules, the RCL is broadly distributed in an ensemble of conformations that cannot be modeled in the electron density, although the general occupancy region can be visualized at low resolution. The most striking feature elucidated by high-resolution refinement of this structure was the presence of an anion-binding site, which was confirmed to contain chloride. Initially, this site was modeled with a water molecule, which refined to the minimum allowed B-factor (2.0 Å^2) and exhibited considerable unaccounted-for electron density (8−12 σ in each of the four copies) in subsequent difference electron density maps (F_o-F_c). This clearly indicated that the occupant of this site had considerably more electron density than a water molecule and was subsequently modeled as a chloride ion, since the crystals were grown in the presence of NaCl. The chloride ion refined to a thermal parameter in keeping with the B factors of the surrounding atoms and showed no additional electron density, positive or negative, in difference maps. The anion's identity was fully confirmed through a substitution experiment, in which a crystal grown in the presence of NaCl was transferred to a solution of NaBr for 5 min, then frozen, and diffraction data collected. Again this site showed considerable unaccounted for electron density despite being modeled as a chloride ion, indicating that the position had been displaced by bromide. These chloride ions are coordinated by four nitrogens, contributed by the protein through two lysine side chains (K323 and K325) and two main chain amides (S149 and H150). The geometry of this binding site is roughly tetrahedral (Table 3). In one of the four molecules in the asymmetric unit, interactions between the chloride ion and both K325 and S149 are displaced with bridging water molecules. This may be related to the rotomer adopted by the side chain of H150, which in this and one other molecule in the asymmetric unit points inward toward the anion binding site and contributes an additional nitrogen ($N_{\delta 1}$) to the coordination of the anion.

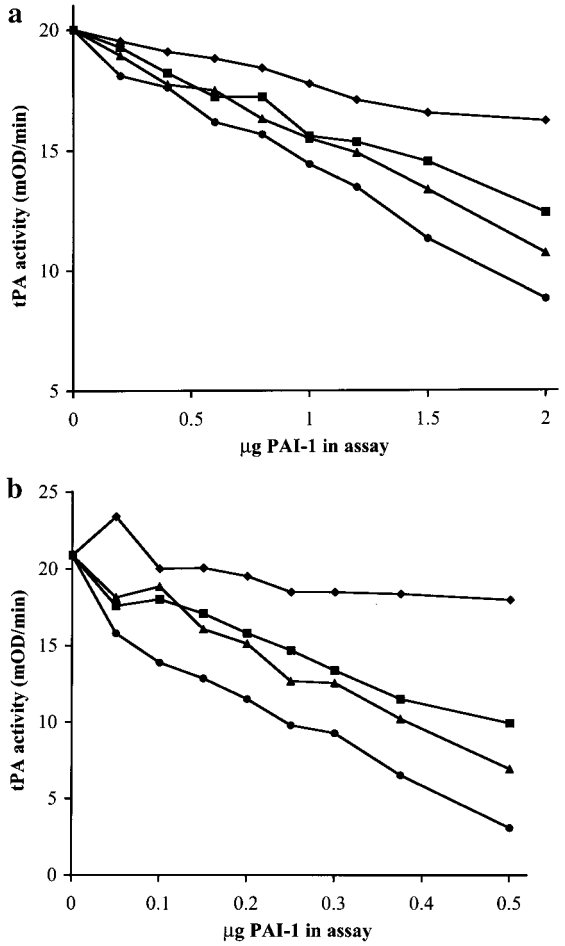

FIGURE 3: Stability of human PAI-1 in the presence of the halide series of anions: (a) Titration of PAI-1 against a fixed concentration of t-PA in the presence of 150 mM NaF, NaCl, NaBr, or NaI, following incubation for 24 h at 25 °C. (b) Titration of PAI-1 against a fixed concentration of t-PA in the presence of 150 mM NaF, NaCl, NaBr, or NaI, following incubation for 30 min at 37 °C. (●) = NaF, (▲) = NaCl, (■) = NaBr, (◆) = NaI.

Stability Modulation by Halides. Results from stability studies are shown in Figure 3. At both temperatures and time points tested, PAI-1 exhibited varying stability depending on the nature of the halide ion present in the incubation buffer. Fluoride appeared to exhibit the greatest stabilizing effect, followed in order by chloride, bromide, and iodide. This trend in stability was consistently observed in multiple experiments with separate preparation and quantitation of the PAI-1/halide stock solutions. Hence, the stability of PAI-1 in the different halide buffers tested appears to be related to the electronegativity and/or ionic radius of the halide present.

DISCUSSION

Latent Conformation of PAI-1. The structure of human PAI-1 in its latent conformation has been previously determined at 2.8 Å resolution, using diffraction data collected at room temperature (*22*). Through a combination of highly purified protein, optimized crystal growth conditions, and the determination of cryogenic conditions, diffraction data were collected from a single crystal to better

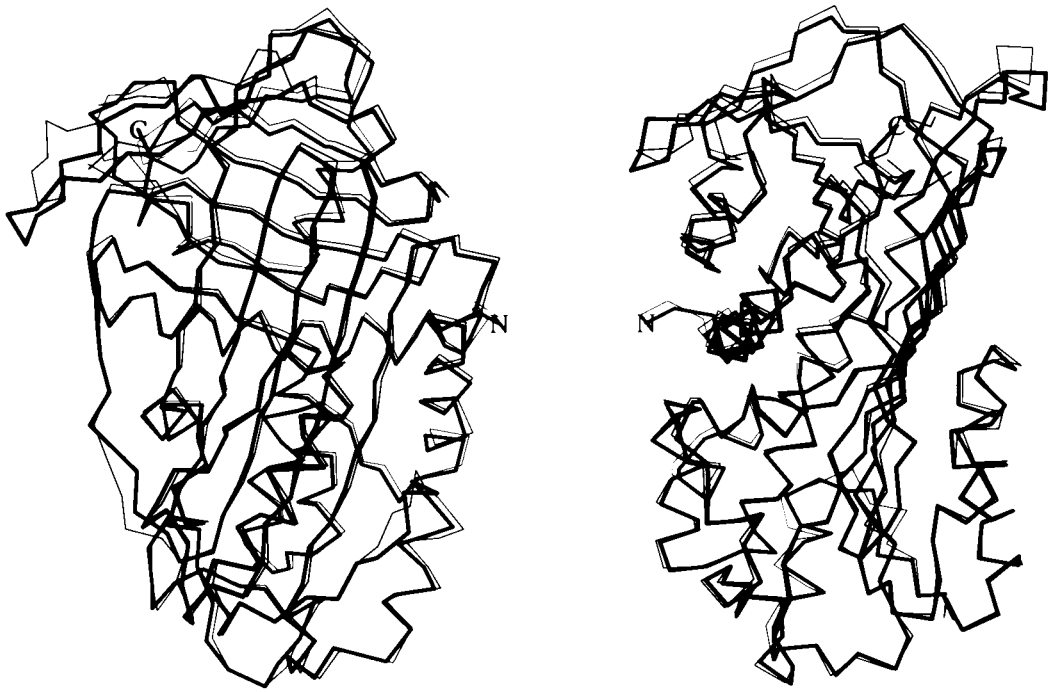

FIGURE 4: Superposition of the room temperature structure of latent PAI-1 as previously published at 2.8 Å (thin lines) with that from this study, measured at −180 °C to 2.1 Å resolution (thick lines). The largest deviations include a loop involved in heparin binding (F113−K122), a stretch of the RCL (A345−E351), and portions of β-sheets B and C including P180−P200, T215−Y221, Y241−P246, and M377−P379. The right-hand figure is rotated 90° relative to the left image.

than 2.0 Å resolution. The structure (Figure 1, right panel) was solved by molecular replacement as described in Materials and Methods. A comparison of this structure to that previously solved (Figure 4) shows that throughout the core of the molecule, the two structures are quite similar; the rmsd on α-carbons of the best fitting subset of 362 residues is 0.62 Å. However, comparing C_α's for the entire protein chain gives an rmsd of 1.39 Å. The largest structural deviations are primarily concentrated in the upper domain of the protein, as illustrated in Figure 2, although smaller improvements to local stereochemistry and chain-tracing are distributed throughout the structure. The upper domain includes β-sheets B and C as well as the C-terminus and is located at the upper rear of the canonical view of the protein structure as depicted in Figure 1, left panel, and Figure 2. In the previous determination of this structure, the upper domain was found to be in general poorly ordered, and it was proposed that this mobility may contribute to the metastability of the active form. In our study, the upper domain is fully located in well-defined electron density and shows no evidence of diffuse disorder. This may be due either to crystals with an inherently higher degree of order or to the collection of diffraction data at cryogenic temperatures that may have served to "freeze-out" thermal motion.

Active Conformation of PAI-1. The structure of PAI-1, stabilized in an active conformation through the introduction of four point mutations, has been solved and refined at 2.4 Å resolution. A moderate resolution (≥3.0 Å) determination of this tetramutant has been recently published (*30*). The two studies used samples with essentially the same crystallographic symmetry: both unit cells contain four independent molecules in space group *P*1 with pseudo-C-centered noncrystallographic symmetry. However, the unit cell dimensions are somewhat different between the two structures, which may be due to either the conditions under which the crystals were grown or perhaps a consequence of differing degrees of conformational heterogeneity. In general, there is a strong positive correlation between the limit of diffraction of a crystalline sample (resolution) and the inherent ordering of the contents of that crystalline lattice. The extended diffraction limits of the crystals used in this study have allowed the determination of additional details of the active conformation of PAI-1.

Stabilizing Mutations. Several relatively stable forms of PAI-1 have been generated by protein engineering, using both random and site-directed mutagenesis strategies (*23*, *25*−*27*). Tucker et al. (*27*) designed a series of mutants with glutamate residues at various positions in the RCL, with the intention of preventing insertion of the loop into the central β-sheet. Several of these mutants exhibited a 10-fold increase in stability. In the same study, mutations in the so-called "gating domain" also produced modest enhancements in stability. (This domain comprises a loop near the C-terminus of PAI-1 over which the RCL must pass during the active-to-latent transition). Lawrence et al. (*26*) found that disruption of a salt bridge between Glu350 and Arg30 (thought to stabilize the latent conformation) caused up to a 2-fold increase in half-life. Sui et al. (*23*) found that mutations of Y221 to histidine and serine gave 2−10-fold stabilization of the active conformation at pH 6.5 but are less stable than wild-type at pH 5.5. This behavior was not seen in the presence of vitronectin (which binds to and stabilizes the active form of PAI-1 in vivo), suggesting that this residue plays a role in the structural transition from the active to the latent form. Most notably, Berkenpas et al. (*25*) used a random mutagenesis approach to identify a tetramutant of PAI-1 that exhibited a 72-fold greater stability than the wild-type protein. While these four mutations are not closely clustered together in three-dimensional space, their effects on the stabilization of PAI-1 are synergistic: the contribu-

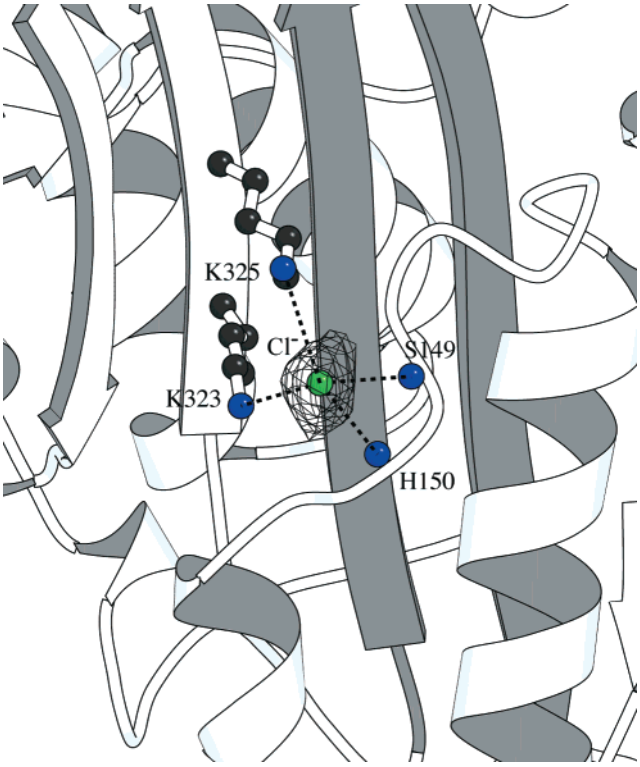

FIGURE 5: Close-up of the anion-binding site. Close hydrogen bonds are made between the chloride ion and four surrounding nitrogens, two of which are contributed by main chain amides (residues 149 and 150) and two by the Nζ of lysines 323 and 325. Details of the geometry of this site are given in Table 3 and in the text. The difference electron density depicted (shown at 5 σ) arises from the bromide-containing data while modeling the anion as a chloride. Any remaining positive electron density in such a calculation is indicative of additional unmodeled electron density.

tions of each of the four mutations are more than additive in the tetramutant (*25*).

As seen in Figure 2, the four mutations that serve to stabilize the active conformation of PAI-1 (N150**H**, K154**T**, Q319**L**, M354**I**) are located in two separate portions of the molecule. One mutation, M354**I**, is located at the C-terminal end of the RCL, which moves in a "jump rope" fashion around the C-terminal face of the protein during the active → latent transition. The other three sites of mutation are somewhat clustered at the base of the primary β-sheet into which the RCL must insert (Figures 1, 2, and 6). One mutation, Q319**L**, replaces a polar residue with a hydrophobic side chain under the small helix−turn−helix subdomain that lies on top of the primary β-sheet. This small domain must fold away from the surface of the β-sheet during the structural transition, much like a hinge. Therefore, the wild-type glutamine may serve to destabilize the buried interface to facilitate this motion. The remaining two mutations, N150**H** and K154**T**, are located within this small "hinge domain" and in two of the independent molecules in the crystal structure form hydrogen-bonding partners. This interaction likely stabilizes the turn of 3_{10}-helix, which, to date, has been found only in the HTLI-PAI-1 structure (*30*).

Stability Modulation through Anion Binding. The unusual lability of the active form of the PAI-1 molecule has prompted a great deal of biochemical investigation. Mutational studies have shown that structural stability can be readily introduced into the protein (*23*, *25*, *26*), which supports the presumption that the functional instability of PAI-1 has evolved as a regulatory element of the fibrinolytic process. Prior to the observation of a PAI-1 crystal structure in its active-form, a considerable amount of biochemical work has focused on the labile nature of PAI-1 and its structural and mechanistic implications (*16*, *18*, *35*, *38*−*45*). A number of factors have been found that accelerate the transition from the active to the latent form, including heat, elevated pH, and certain buffers (*21*, *46*) (D.I.B., unpublished results). The stabilizing role of sodium chloride, however, has not been elaborated beyond the empirical observations that it (i) promotes solubilization of the PAI-1 protein and (ii) engenders additional stability to the active form. The additional detail revealed in the two high-resolution crystal structures reported here has provided a structural interpretation for the role of physiological salt in the mechanism of action of human PAI-1.

After the first cycles of refinement of HTLI-PAI-1, it became immediately clear that there was significant unaccounted-for density in all four molecules of HTLI-PAI-1 located between the central β-sheet and the small "hinge" domain. These peaks ranged from 7 to 15 σ and were initially modeled as water molecules. Subsequent refinement led to additional unmodeled electron density at these positions, as well as thermal parameters for the water molecules, which had refined to the smallest allowed value (2.0 Å^2). These are both characteristics of the presence of a more electron-dense element than that included in the atomic model. It was also observed that this peak position was fully ligated by nitrogens (the N_ζ's of lysines 323 and 325 and the two main chain amides of S149 and H150), indicating that this position was an anion-binding site. Since the crystallization medium contained only 1 M NaCl and 20 mM MES, chloride was considered as the only likely anion. Replacement of the four water molecules with four chloride ions promptly led to thermal parameters that were in line with the thermal parameters of the surrounding protein atoms and no additional unmodeled electron density in subsequent difference maps. This identification was further confirmed through the collection of an additional data set for which a crystal of HTLI-PAI-1 was moved from its growth mother liquor into a solution containing 2 M NaBr and 35% ethylene glycol. The crystal was allowed to soak for 5 min before transfer into the N_2 cold stream for data collection. As shown in Figure 5, additional electron density resulted at the chloride positions, confirming the substitution of bromide ions at the anion-binding site.

Since the anion-binding site sits directly between strand 5A of the central β-sheet and the hinge domain, forming close interactions with each side (Figure 5) and directly in the presumed path of the inserting RCL during the active → latent structural transition, we considered whether the nature of the anion had an effect on the structural lability of PAI-1. Freshly prepared samples of wt PAI-1 were buffer-exchanged into 150 mM solutions of NaF, NaCl, NaBr, and NaI at pH 7.4, allowed to incubate at 4 and 25 °C for 0, 1, 2, 4, 8, 18, and 25 h, and assayed for the ability to inhibit t-PA. This "stability assay" showed a clear trend (Figure 3) corresponding to the electronegativity of the halide present. At 25 °C, the half-life of the active form of PAI-1 progresses with the increasing electronegativity of the anion, i.e., $I^- < Br^- < Cl^- \leq F^-$. This is likely due to the increasingly

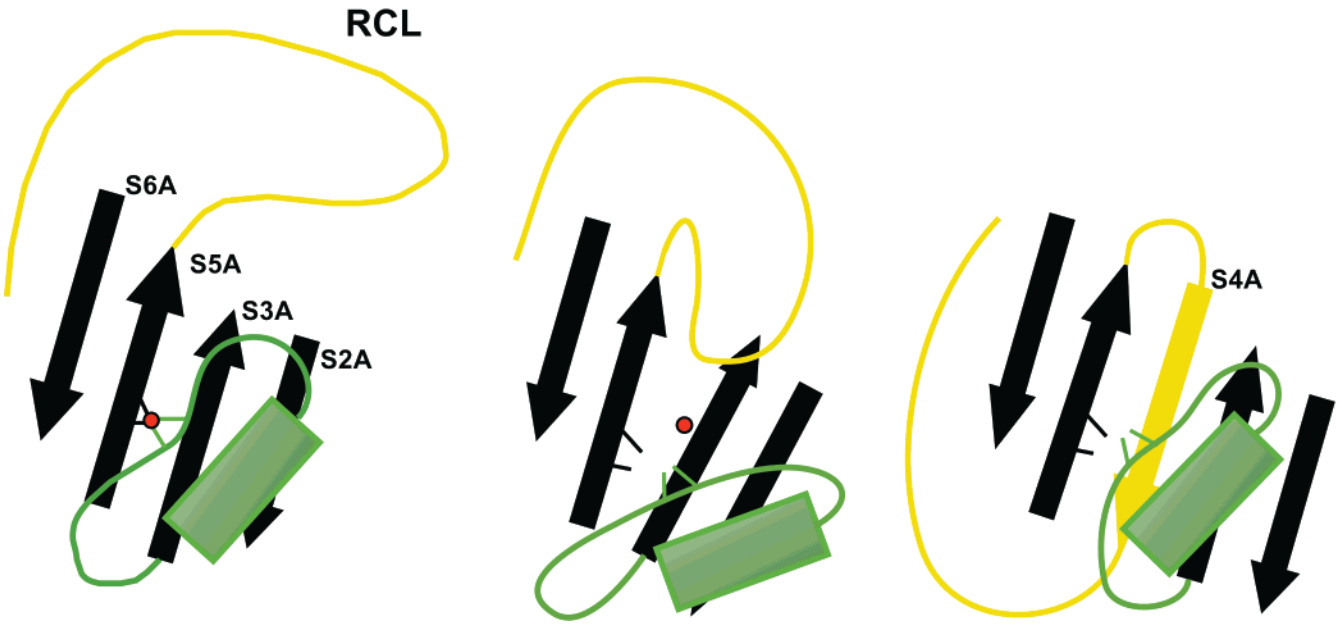

FIGURE 6: Cartoon depiction of the proposed role of the anion-binding site in the structural transition from the active (left) to the latent (right) form of human PAI-1. The RCL is shown in yellow, while the "hinge domain" is shown in green. The anion is shown in red. The ionic interaction bridged by the anion between the hinge domain and strand 5A of the central β-sheet must be dissociated (center) for the RCL to fully insert into β-sheet A and produce the uncleaved latent form.

electronegative ions forming stronger interactions with the partially positive nitrogens of the anion-binding site. Since the hinge domain must detach from the surface of the central β-sheet and swing away to allow entry of the RCL into the β-sheet during the active → latent transition, a tighter interaction should serve to increase the energy barrier to this transition, a trend that is reflected in this series of assays. While this is not a profound effect, it does reflect the exquisite sensitivity with which processes such as the fibrinolytic cascade are regulated. It has been observed (D.I.B., unpublished results) that removal of monovalent anion salts from solutions of PAI-1 leads to rapid aggregation and precipitation of the protein, clearly an undesired behavior within the circulatory system.

The possibility cannot be excluded, however, that we have observed a coincidental halide-binding site located in the direct path of the active to latent structural transition of human PAI-1 and that the above stabilization of active wild-type PAI-1 by the sodium salts of the halides simply reflects some general protein stabilization effect (*47*). An important question is whether the conformation of the 3_{10}-helix and adjacent area is (i) induced by the stabilizing mutations H150 and T152, (ii) induced by the binding of anions, or (iii) is an intrinsic feature of the active conformation of PAI-1. All of the structures of HTLI-PAI-1 determined to date, whether bound with anions in the binding site or not, show the same conformation of this 3_{10}-helix and adjacent loop; conformation induced by anion-binding is therefore unlikely. Other serpins whose structures have been determined do not contain this short stretch of 3_{10}-helix; however, only PAI-1 displays intrinsic structural metastability. In the absence of a structure of active, wild-type PAI-1, we do not believe that there is enough evidence to make a confident assertion as to whether this local conformation is intrinsic to the active conformation of PAI-1 or induced by the stabilizing mutations. In either case, the question is sufficiently compelling to prompt further investigation.

CONCLUSIONS

Serpins form a general class of proteinaceous protease inhibitors that function by presenting a bait-like extended loop to the target protease. Following the initial binding event, a covalent attachment is formed between the reactive serine and the main-chain of the inhibitor, and the covalent complex undergoes a structural transition into an extraordinarily stable form. Human PAI-1 exists physiologically in a metastable active form, which rapidly converts to an inactive form through an extensive structural rearrangement. This inactive form is generally referred to as "latent", since activity can be restored through denaturing and refolding; however, under physiological conditions, no activity toward t-PA is recovered once the transition has occurred.

The observation of an anion-binding site in human PAI-1 and its apparent role in the modulation of the active form of this serpin raises the question of generality: is this found in all serpins or more specifically in all PAI-1's? Clearly, since PAI-1 is anomalous among serpins with regard to the metastability of its active form, this type of active form modulator would not be expected to be found among general serpins. Indeed, sequence alignments show that, in general, lysine 323 and, in particular, lysine 325 are not conserved among other serpins such as antitrypsin, antithrombin, antiplasmin, C1-esterase inhibitor, maspin, and PAI-2. In contrast, although we do not currently have biophysical data on the metastability of PAI-1's from other mammalian species, one would expect that this anion-binding site should be preserved. Indeed, by sequence alignment, lysines 323 and 325 are completely conserved among PAI-1's from human, mink, rat, mouse, cow, and pig, with the singular conservative substitution of K325 → R in mouse.

In conclusion, the availability of high-resolution crystallographic data on these forms of human PAI-1 has revealed a structural role for chloride ions in this key component of the fibrinolytic pathway. The anion-binding site sits between

two domains that must separate during the active → latent structural transition. We propose that the chloride ion may act as a displaceable "pin", helping to maintain PAI-1 in an active form but allowing the removal of PAI-1 activity when required. Although our data do not conclusively demonstrate that this effect is physiologically relevant to wild-type PAI-1 activity, we believe that the evidence is sufficiently compelling to warrant further investigation. We envision additional studies to probe the importance of this anion-binding site through mutagenesis; in particular, mutations at lysines 323 and 325 should be instructive. Key questions that remain include further characterization of the energetics of the interaction of halides with the anion binding site, whether this modulation is conserved among PAI-1's from other species, and the possible role of this site in the stabilization of the PAI-tPA product after the acyl−enzyme complex has been formed.

ACKNOWLEDGMENT

We thank Carleton Sage, Glenn Hammonds, and Art Hanel for fruitful discussions, as well as Michael Wang for preparation of the PAI-1 plasmid. We also thank Elizabeth Goldsmith for sharing the latent-PAI coordinates and the support of our colleagues at Eli Lilly & Co.

REFERENCES

1. Sprengers, E. D., and Kluft, C. (1987) *Blood 69*, 381−387.
2. Alessi, M. C., Declerck, P. J., De Mol, M., Nelles, L., and Collen, D. (1988) *Eur. J. Biochem. 175*, 531−540.
3. Loskutoff, D. J., Sawdey, M., and Mimuro, J. (1989) *Prog. Hemostasis Thromb. 9*, 87−115.
4. Danø, K., Andreasen, P. A., Grondahl-Hansen, J., Kristensen, P., Nielsen, L. S., and Skriver, L. (1985) *Adv. Cancer Res. 44*, 139−266.
5. Huber, K., and Carrell, R. W. (1989) *Biochemistry 28*, 8951−8966.
6. Pannekoek, H., Veerman, H., Lambers, H., Diergaarde, P., Verweij, C. L., van Zonneveld, A. J., and van Mourik, J. A. (1986) *EMBO J. 5*, 2539−2544.
7. Ny, T., Sawdey, M., Lawrence, D., Millan, J. L., and Loskutoff, D. J. (1986) *Proc. Natl. Acad. Sci. U.S.A. 83*, 6776−6780.
8. Ginsburg, D., Zeheb, R., Yang, A. Y., Rafferty, U. M., Andreasen, P. A., Nielsen, L., Dano, K., Lebo, R. V., and Gelehrter, T. D. (1986) *J. Clin. Invest. 78*, 1673−1680.
9. Andreasen, P. A., Riccio, A., Welinder, K. G., Douglas, R., Sartorio, R., Nielsen, L. S., Oppenheimer, C., Blasi, F., and Danø, K. (1986) *FEBS Lett. 209*, 213−218.
10. Kvassman, J. O., Verhamme, I., and Shore, J. D. (1998) *Biochemistry 37*, 15491−15502.
11. Wilczynska, M., Fa, M., Ohlsson, P. I., and Ny, T. (1995) *J. Biol. Chem. 270*, 29652−29655.
12. Lawrence, D. A., Ginsburg, D., Day, D. E., Berkenpas, M. B., Verhamme, I. M., Kvassman, J. O., and Shore, J. D. (1995) *J. Biol. Chem. 270*, 25309−25312.
13. Lindahl, T. L., Ohlsson, P. I., and Wiman, B. (1990) *Biochem J. 265*, 109−113.
14. Fa, M., Karolin, J., Aleshkov, S., Strandberg, L., Johansson, L. B., and Ny, T. (1995) *Biochemistry 34*, 13833−13840.
15. Stromqvist, M., Karlsson, K. E., Bjorquist, P., Andersson, J. O., Bystrom, M., Hansson, L., Johansson, T., and Deinum, J. (1996) *Biochim. Biophys. Acta 1295*, 103−109.
16. Declerck, P. J., De Mol, M., Vaughan, D. E., and Collen, D. (1992) *J. Biol. Chem. 267*, 11693−11696.
17. Urano, T., Strandberg, L., Johansson, L. B., and Ny, T. (1992) *Eur. J. Biochem. 209*, 985−992.
18. Sancho, E., Declerck, P. J., Price, N. C., Kelly, S. M., and Booth, N. A. (1995) *Biochemistry 34*, 1064−1069.
19. Gils, A., Knockaert, I., and Declerck, P. J. (1996) *Biochemistry 35*, 7474−7481.
20. Levin, E. G., and Santell, L. (1987) *Blood 70*, 1090−1098.
21. Lindahl, T. L., Sigurdardottir, O., and Wiman, B. (1989) *Thromb. Haemostasis 62*, 748−751.
22. Mottonen, J., Strand, A., Symersky, J., Sweet, R. M., Danley, D. E., Geoghegan, K. F., Gerard, R. D., and Goldsmith, E. J. (1992) *Nature 355*, 270−273.
23. Sui, G. C., and Wiman, B. (1998) *FEBS Lett. 423*, 319−323.
24. Gils, A., Lu, J., Aertgeerts, K., Knockaert, I., and Declerck, P. J. (1997) *FEBS Lett. 415*, 192−195.
25. Berkenpas, M. B., Lawrence, D. A., and Ginsburg, D. (1995) *EMBO J. 14*, 2969−2977.
26. Lawrence, D. A., Olson, S. T., Palaniappan, S., and Ginsburg, D. (1994) *Biochemistry 33*, 3643−3648.
27. Tucker, H. M., Mottonen, J., Goldsmith, E. J., and Gerard, R. D. (1995) *Nat. Struct. Biol. 2*, 442−445.
28. Kvassman, J. O., Lawrence, D. A., and Shore, J. D. (1995) *J. Biol. Chem. 270*, 27942−27947.
29. Keijer, J., Linders, M., Klein Gebbick, R., Ehrlich, H. J., and Pannekoek, H. (1990) *Fibrinolysis 4*, 153−159.
30. Sharp, A. M., Stein, P. E., Pannu, N. S., Carrell, R. W., Berkenpas, M. B., Ginsburg, D., Lawrence, D. A., and Read, R. J. (1999) *Struct. Fold Des. 7*, 111−118.
31. Sancho, E., Tonge, D. W., Hockney, R. C., and Booth, N. A. (1994) *Eur. J. Biochem. 224*, 125−134.
32. Kvassman, J.-O., and Shore, J. D. (1995) *Fibrinolysis 9*, 215−221.
33. Otwinowski, Z. (1993) in *Proceedings of the CCP4 Study Weekend: "Data Collection and Processing"* (Sawyer, L., Isaacs, N., Bailey, S., Eds.) pp 56−62, SERC Daresbury Laboratory, England.
34. Brünger, A. T. (1996) X-PLOR.
35. Sui, G. C., and Wiman, B. (1998) *Biochem. J. 331* (Pt 2), 409−415.
36. Ehrlich, H. J., Gebbink, R. K., Keijer, J., and Pannekoek, H. (1992) *J. Biol. Chem. 267*, 11606−11611.
37. Björquist, P., Ehnebom, J., Inghardt, T., Hansson, L., Lindberg, M., Linschoten, M., Strömqvist, M., and Deinum, J. (1998) *Biochemistry 37*, 1227−1234.
38. Karolin, J., Fa, M., Wilczynska, M., Ny, T., and Johansson, L. B. (1998) *Biophys. J. 74*, 11−21.
39. Schulze, A. J., Quarzago, D., and Andreasen, P. A. (1996) *Eur. J. Biochem. 240*, 550−555.
40. Kjoller, L., Martensen, P. M., Sottrup-Jensen, L., Justesen, J., Rodenburg, K. W., and Andreasen, P. A. (1996) *Eur. J. Biochem. 241*, 38−46.
41. Engh, R. A., Huber, R., Bode, W., and Schulze, A. J. (1995) *Trends Biotechnol. 13*, 503−510.
42. Gils, A., and Declerck, P. J. (1998) *Thromb. Haemostasis 80*, 286−291.
43. Gils, A., and Declerck, P. J. (1997) *J. Biol. Chem. 272*, 12662−12666.
44. Vaughan, D. E., Declerck, P. J., Reilly, T. M., Park, K., Collen, D., and Fasman, G. D. (1993) *Biochim. Biophys. Acta 1202*, 221−229.
45. Wang, Z., Mottonen, J., and Goldsmith, E. J. (1996) *Biochemistry 35*, 16443−16448.
46. Reilly, T. M., Seetharam, R., Duke, J. L., Davis, G. L., Pierce, S. K., Walton, H. L., Kingsley, D., and Sisk, W. P. (1990) *J. Biol. Chem. 265*, 9570−9574.
47. Baldwin, R. L. (1996) *Biophys. J. 71*, 2056−63.

BI000290W